FINITE ELEMENT-BASED COMPRESSION SIMULATION AND PERMEATION PERFORMANCE MEASUREMENT AND CONTROL OF HIGH TEMPERATURE SEALING MATERIALS

Lifang CHEN [1*], Yixiang GUO [2]

To obtain the characteristic operational parameters of spacecraft heat seals, a customized tester is used to carry out the structure and performance research of the P-shaped heat seals. A heat-sealing test system is built to simulate real working conditions. The structure and the plan of the tester are optimized based on the finite element thermal analysis method. For different compression rates and pore-opening structures, the leakage rates of the P-shaped seal are tested at room temperature, high temperature, and different air pressures. The test results show that the leakage of the P-shaped sealing ring decreases with the increase of compression rate and the number of openings on the outer high-pressure side. These results are following those of the finite element theoretical analysis. The main control factors that affect the size of seal leakage have been preliminarily determined, and the data obtained from the test has laid the foundation for future research on sealing theory.

Keywords: heat sealing, leakage rate, P-shaped sealing, finite element simulation, testing technology

1. Introduction

Thermal protection is one of the critical technologies for the development of hypersonic and reusable aircraft. The high temperature and long-term heat sealing of the fuselage openings (such as hatch and landing gear) are essential parts of the thermal protection system [1,2]. The high-temperature seals should ensure both

[1] Key Lab of Engine Health Monitoring Control and Networking of Ministry of Education, Beijing University of Chemical Technology, Beijing 100029, China
[2] State Key Laboratory of High-end Compressor and System Technology, Beijing University of Chemical Technology, Beijing 100029, China
Corresponding author.E-mail addresses: chenlf@mail.buct.edu.cn

good and matching performance of the hatch in the working process, such as heat insulation, leakage protection, strength, and ensure uniform force in opening and closing the hatch. Once the seals fail, hot air will penetrate the fuselage's force-bearing structure and thus enter the body, causing catastrophic consequences [3,4]. For example, the Challenger and Columbia space shuttle accidents all had heat seal failure problems [5,6].

When designing high-temperature seals, performance calibration of high-temperature heat seals using test trials is essential in developing heat seals. After the Columbia crash, NASA carried out many heat seal structures and performed experimental research from the end of the 20th century to the beginning of the 21st century [7-11]. Aiming at the proper heat sealing of the landing gear door of the space shuttle, comparative tests were conducted to analyze the effects of compressibility, dipping layer, structural grooves, and openings of seals on the sealing performance [12,13]. However, most tests were carried out at room temperature, while high-temperature environmental tests were lacking [14-16]. Research on heat sealing mostly focuses on simulation and testing of leakage and thermal transfer in China, and (to the best knowledge of the authors), there is no research on high-temperature heat sealing tests [17-20].

With the development of hypersonic aircraft technology, it became essential to carry out heat-sealing targeted test research to improve the sealing performance and the structural design [21-24]. However, the working conditions of high-temperature seals for aircraft are complex and changeable. Moreover, it is difficult to obtain precisely the same condition among tests, which also brings difficulties to the high-temperature seal performance calibration and verification.

This paper proposes a heat-sealing structure and performance test technology that combines finite element simulation and experimental tests in response to this situation. Taking the P-shaped seals for the cabin door as an example, the finite element thermal transfer and flow simulation results are used to improve the experimental device and the test plan. In this way, matched simulated working conditions are obtained, ensuring that the heat-sealing test results are closer to real working conditions.

2 Heat Sealing Test System

2.1 Test principle and system

To conduct the structure and performance testing of the above-mentioned high-temperat-ure seals under different temperatures, compression rates, and

structures, it is necessary to measure the temperature and pressure of the gas entering the heat seal, flow rate, and temperature of the leaking gas in real-time. The schematic representation of the test principle is shown in Fig. 1.

The test system is built according to Fig. 2, which includes a hot air system (including air compressors, regulating valves, hot air tunnels, pressure gauges, etc.), heat sealing test devices (including temperature and air pressure sensors), flow meters for leakage test, software and hardware control systems and other parts.

(1) Hot air with adjustable pressure and temperature: An air compressor is installed in front of the hot wind tunnel. The pressure can be adjusted by controlling the flow rate using the regulating valve. The hot wind tunnel uses a finned dry-burning heater, which can provide hot air with a temperature up to 1000°C to simulate the hot air flow generated by the high-speed air friction of the spacecraft.

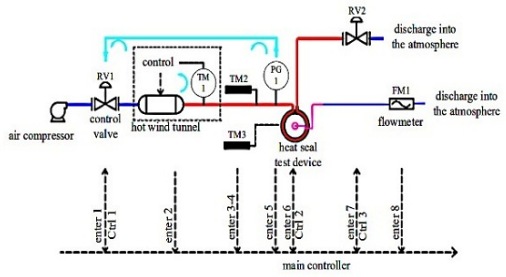

Fig.1. Heat sealing test principle

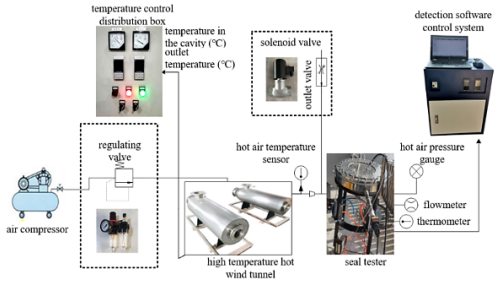

Fig.2. Heat sealing test system

(2) High-temperature environment: The top of the heat sealing test device is directly heated by the high-temperature backplane, and the heat source is a nickel-chromium alloy mica heater. The contact position of the sealing ring is directly heated to the target temperature (such as 200°C), and the temperature is controlled to simulate the real thermal environment.

(3) Control system and computer software: PLC control system is used to access the sensors of each temperature measurement point, pressure sensors, and control valves. The control and monitoring interface of the computer software is presented in Fig. 3, which can supervise the hot air temperature, the temperature of the sealing ring backplane, leakage volume, gas pressure, and leakage gas temperature in real-time.

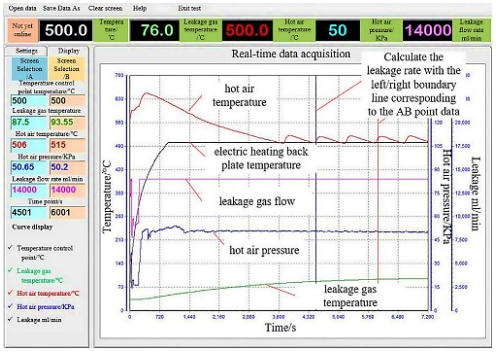

Fig.3. High-temperature heat sealing test software

(4) Heat sealing tester: The heat seal to be tested (taking the P-shaped ring as an example) is installed in the sealing tester. The output parameters are monitored in real-time by the measurement and control system equipped with software developed by ourselves. In the system, the PLC acts as the bridge to communicate with the computer and other devices so that the computer can obtain the temperature and flow rate of the leaking gas. Data generated in the test process can be read and recorded accurately by the computer software in real-time. The structure and working principle of the tester are shown in Fig. 4.

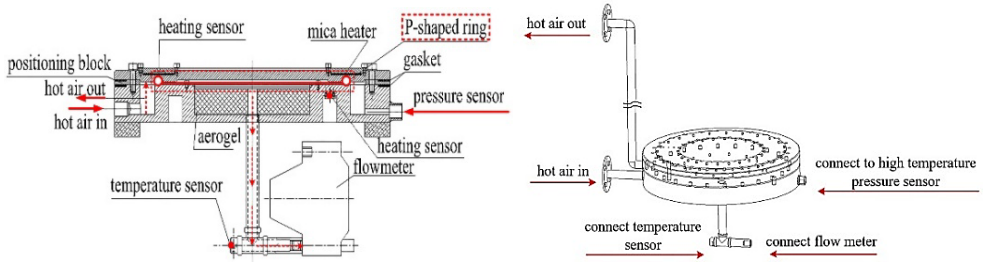

(a) The heat-sealing tester (b) The whole heat-sealing test system

Fig.4. Tester structure and working principle

2.2 Structure and performance simulation

2.2.1 Analysis of the temperature field of the tester

Heat seals are the main barriers to isolate the spacecraft cabin from the outside world. The heat transfer analysis of the tester body is fundamental because of the high-temperature hot air required for the test. Considering the steady-state and transient local heating generated by the high-speed motion of the spacecraft, as well as the aerodynamic loads and high fluctuating pressure loads, it is necessary for the high-temperature seals to reach and withstand the operating temperatures and to stay stable under the demanding parameters to ensure that the normal function of the seals. Therefore, the finite element steady-state thermal and transient

thermal analysis of the tester body is used to predicate whether the tester can work under the target temperature (hot airflow temperature 250 °C, backplate rubber ring heated to 200 °C), and the field test can be carried out successfully.

The general equation of steady-state thermodynamic analysis is [25]:

$$[\boldsymbol{K}]\{\boldsymbol{I}\}=\{\boldsymbol{Q}\} \tag{1}$$

where [$\boldsymbol{K}$] is the conduction matrix, including thermal coefficients, convection coefficients, radiation coefficients, and shape coefficients; {$\boldsymbol{I}$} is the node temperature vector; {$\boldsymbol{Q}$} is the node heat flow vector, including heat generation.

The general equation of transient thermodynamic analysis is [25]:

$$[\boldsymbol{C}]\{\dot{\boldsymbol{T}}\}+[\boldsymbol{K}]\{\boldsymbol{T}\}=\{\boldsymbol{Q}\} \tag{2}$$

where [$\boldsymbol{K}$] is the conduction matrix, [$\boldsymbol{C}$] is the specific heat matrix, {$\boldsymbol{T}$} is the node temperature vector, { $\dot{\boldsymbol{T}}$ } is the derivative of node temperature concerning time, {$\boldsymbol{Q}$} is the node heat flow vector, including heat generation.

The heat flow in the tester mainly transfers in conduction, which exchanges heat between the wall of the tester and the P-shaped sealing ring to be tested. The heat conduction follows Fourier's law, as shown in Equation (3). For the analysis of thermal structure, the two-dimensional thermal conductivity control differential equation [26] is defined in Equation (4).

$$q'' = -k\frac{\mathrm{dT}}{\mathrm{dx}} \tag{3}$$

where q'' is the heat flux (W/m^2); k is the thermal conductivity (W/(m·°C)).

$$\rho c\frac{\partial T}{\partial \theta}=\lambda(\frac{\partial^2 T}{\partial x^2}+\frac{\partial^2 T}{\partial y^2}) \tag{4}$$

In the above equation, the left side is the increment of the thermodynamic energy of the solid micro-element, and the right side is the net heat flow introduced into the micro-element. Furthermore, T is the temperature; c is the heat capacity; λ is the thermal conductivity; θ is the time increment.

Some conditional parameters of finite element simulation analysis are shown in Table 1 [27].

The calculation is made simpler by using the shortened 1/24 model as the analysis object (axisymmetric model). The base, the upper gland, the mica upper gland, the attaching bolts, the mica sheet, the base insulation plate, and the aerogel make up the model's main construction. The overall grid size is 2-3 mm, and the hexahedron-based finite element grid is produced. The major components are

locally densed in order to further acquire more precise simulation results. In Figure 5, the precise grid division is displayed.

Table 1

Parameters of structural parts

Structural parts	Elastic Modulus /Pa	Poisson's ratio	Isotropic thermal conductivity /W·m^{-1}·°C^{-1}	Specific heat capacity /J·kg^{-1}·°C^{-1}
Heater base, heater, upper gland, phlogopite upper gland, bolt	2E11	0.3	60.5	434
Phlogopite	1.5E9	0.23	0.34	500
Base insulation board	7.3E10	0.22	1.4	750
Aerogel	5E6	0.32	0.033	502.08

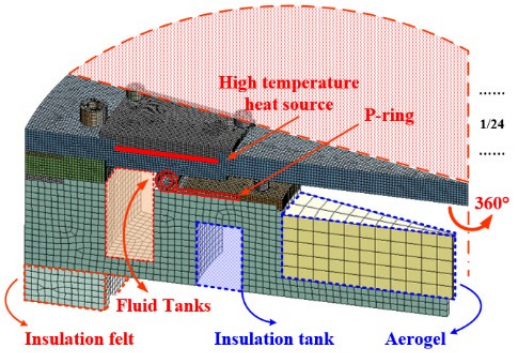

Fig.5. Meshing diagram of the 1/24 model of the tester

For the overall model, the total number of cells is 51065 and the total number of nodes is 218523. The mean value of total mesh mass 0.826 is greater than the empirical value 0.7, which is verified by mesh irrelevance and meets the calculation accuracy requirements.

The simulation calculation results show that the highest temperature is in the heated area in the upper part of the backplane, while the lowest temperature is in the middle aerogel leakage path area, and the calculation cloud diagram is shown in Figure 6. In order to simulate the real working environment, an insulation slot is added at the bottom to separate the hot air outer cavity from the leaking inner cavity. The inner cavity is filled with aerogel.

According to the analysis results, the 900s tester structure can satisfy the 200 ℃ test temperature according to the calculation of a single heat source condition of 200 ℃. The highest temperature is 199.86 °C, which occurs at the upper surface (sealing surface) of the P-shaped rubber ring, while the temperature of the bottom surface is lower (155.36 °C). This ensures that the test can be continued smoothly.

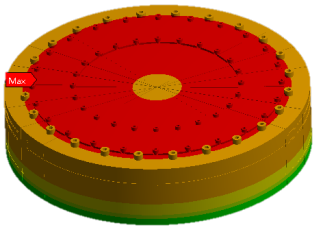

(a) The overall structure analysis result of the tester

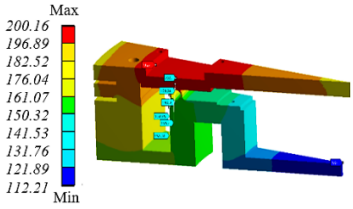

(b) Thermal analysis results of the 1/24 model

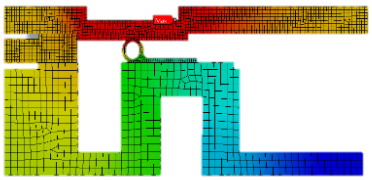

(c) 2D cross-sectional view of the transient thermal analysis of tester

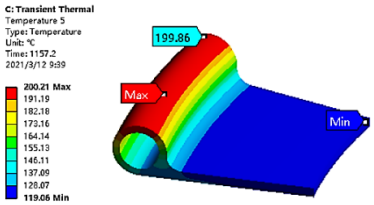

(d) Transient thermal analysis results of the P-shaped ring

Fig.6. Cloud images of thermodynamic analysis results of the tester

2.2.2 Compression deformation simulation of the test piece

In the sealing leakage test, it is necessary to investigate the impact of different compression rates of the P-shaped ring. The sealing process adopts the means of close contact to minimize the leakage of external airflow. The equivalent stress and strain values of the contact sealing position are calculated by finite element simulation, and then the heat-sealing performance of the P-shaped ring is evaluated. The compression rate of the sealing ring is defined following the calculation method specified in JB T9141.4-1999 [28]. The thickness before and after compression is recorded, and the compression rate is calculated as:

$$C = \frac{t_0 - t_1}{t_0} \times 100\% \tag{5}$$

where C is the compression rate, t_0 and t_1 are the thickness (in mm) of the sample before and after compression, respectively.

We use three types of P-shaped rubber ring test pieces. The first type has an 11 mm outer diameter, the second type has a 22mm outer diameter, and the third type also has a 22mm outer diameter, but the outer ring has different numbers of bottom holes. All three types of rubber seals are made of No. 6051 rubber, which has undergone hardness test, tensile strength test, tensile strength test, tensile elongation test, and tensile permanent deformation test at the factory. This space-grade sealing material has good adaptability to the space environment, excellent vacuum, and UV resistance, and charged particle radiation performance, thus satisfying the basic parameter requirements of the test. One P-shaped rubber ring sample is shown in Fig. 7.

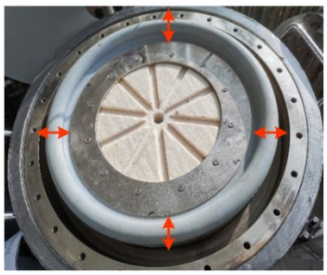

(a) P-shaped ring with 22mm diameter

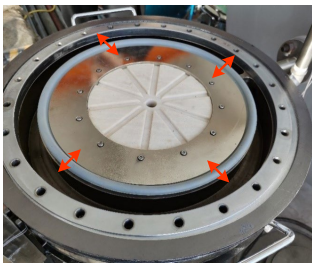

(b) P-shaped ring with 11mm diameter

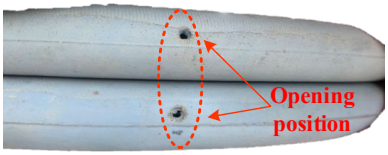

(c) P-shaped ring with 22mm diameter (4 holes)

(d) P-shaped ring with 22mm diameter (8 holes)

Fig.7. P-shape sealing rings to be tested

The P-shaped rings are made of rubber. R-ubber is a super-elastic material with good flexibility and resilience. It is widely used in sealing and damping. The characteristics of rubber materials are intricate. Their physical and chemical properties are very different from those of metal materials, mainly reflected in rubber materials' triple nonlinearity (geometry, material, and boundary nonlinearity), significant deformation characteristics, and incompressibility. Although rubber materials are generally simulated as incompressible, their bulk modulus is not infinite. In most applications, using the relative incompressible model and the compressible model will not make a big difference [29-32]. Therefore, finite element analysis is used to investigate the compression deformation of the rubber ring, by which the equivalent stress and equivalent strain are obtained. The sealing performance of the rubber ring is analyzed and evaluated to avoid permanent failure of the seal due to excessive deformation caused by yielding [33-36].

The equivalent expression of Von Mises stress is shown in Equation (6). Calculating the equivalent total strain from the elastic, plastic, thermal, and creep stresses [37]. The Ogden model is based on the principal tension of the left Cauchy-Green tensor, where the strain potential is shown in Equation (7). The expression of the Cauchy stress under compression in the laboratory is as Equation (8).

$$\boldsymbol{\sigma} = \left\{ \left[(\boldsymbol{\sigma}_1 - \boldsymbol{\sigma}_2)^2 + (\boldsymbol{\sigma}_2 - \boldsymbol{\sigma}_3)^2 + (\boldsymbol{\sigma}_3 - \boldsymbol{\sigma}_1)^2 \right] / 2 \right\}^{\frac{1}{2}} \tag{6}$$

where are the principal stresses in the three directions of the unit body.

$$W = \sum_{i=1}^{N} \frac{\mu_i}{\alpha_i} \left(\overline{\lambda}_1^{\alpha_i} + \overline{\lambda}_2^{\alpha_i} + \overline{\lambda}_3^{\alpha_i} - 3 \right) + \sum_{k=1}^{N} \frac{1}{d_k} (J-1)^{2k} \tag{7}$$

where W is the strain potential energy; $\overline{\lambda}_{\mathrm{p}}(\mathrm{p}=1,2,3)$ is the principal deviation stretch, which is defined as $\overline{\lambda}_p = J^{-\frac{1}{3}}\lambda_p$; λ_{p} is the principal stretch of the left Cauchy-Green tensor; J is the determining factor of the elastic deformation gradient; N, μ_{p}, a_{p} and d_{p} are the material constants, and usually there is no limitation on N.

$$\boldsymbol{\sigma}_{11}=2\left(\lambda_1^2-\frac{1}{\lambda_2}\right)\left(\frac{\partial W}{\partial \boldsymbol{I}_1}+\frac{1}{\lambda_1}\frac{\partial W}{\partial \boldsymbol{I}_2}\right) \tag{8}$$

where $\boldsymbol{I}_1$ is the unit tensor, λ is the principal elongation, and W is the strain energy function.

A qualitative analysis of the assembly structure is conducted. To simplify the calculations, static analysis of the 2D cross-section is used in ANSYS. The calculation mesh model is shown in Fig. 8. Two P-shaped ring sizes (outer diameter of 22mm and 11mm) and eight compression rates (1%, 4%, 6%, 10%, 15%, 20%, 25%, and 42%) are used in the simulation. The cloud images corresponding to compression rates of 10%, 20%, and 42% are presented in Fig. 9.

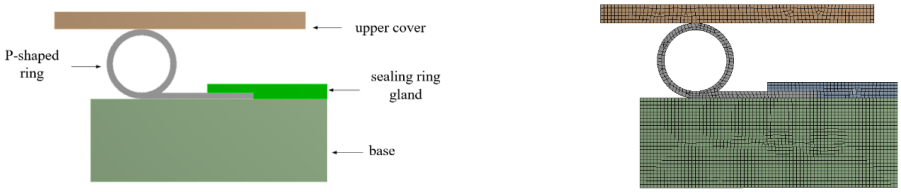

Fig.8. Simplified calculation model and mesh division

The compression distance and compression rate setup, as well as the simulation results for the two sizes of P-shaped rings, are collected in Table 2:

Table 2

Simulation results of sealing ring compression

11mm P-shaped sealing ring	Group 1	Group 2	Group 3	Group 4	Group 5	Group 6	Group 7	Group 8
Compression rate /%	1	4	6	10	15	20	25	42
Compression distance/mm	0.11	0.44	0.66	1.1	1.65	2.2	2.75	4.62
Equivalent stress /MPa	0.01	0.04	0.059	0.099	0.32	0.39	0.47	0.78
Equivalent strain /mm	0.0034	0.0133	0.0199	0.033	0.05	0.06	0.08	0.13
22mm P-shaped sealing ring	Group 1	Group 2	Group 3	Group 4	Group 5	Group 6	Group 7	Group 8
Compression rate /%	1	4	6	10	15	20	25	42
Compression distance/mm	0.22	0.88	1.32	2.2	3.3	4.4	5.5	9.24
Equivalent stress /MPa	0.0068	0.0887	0.093	0.17	0.106	0.172	0.178	0.275
Equivalent strain /mm	0.0023	0.03	0.0315	0.06	0.036	0.06	0.062	0.0958

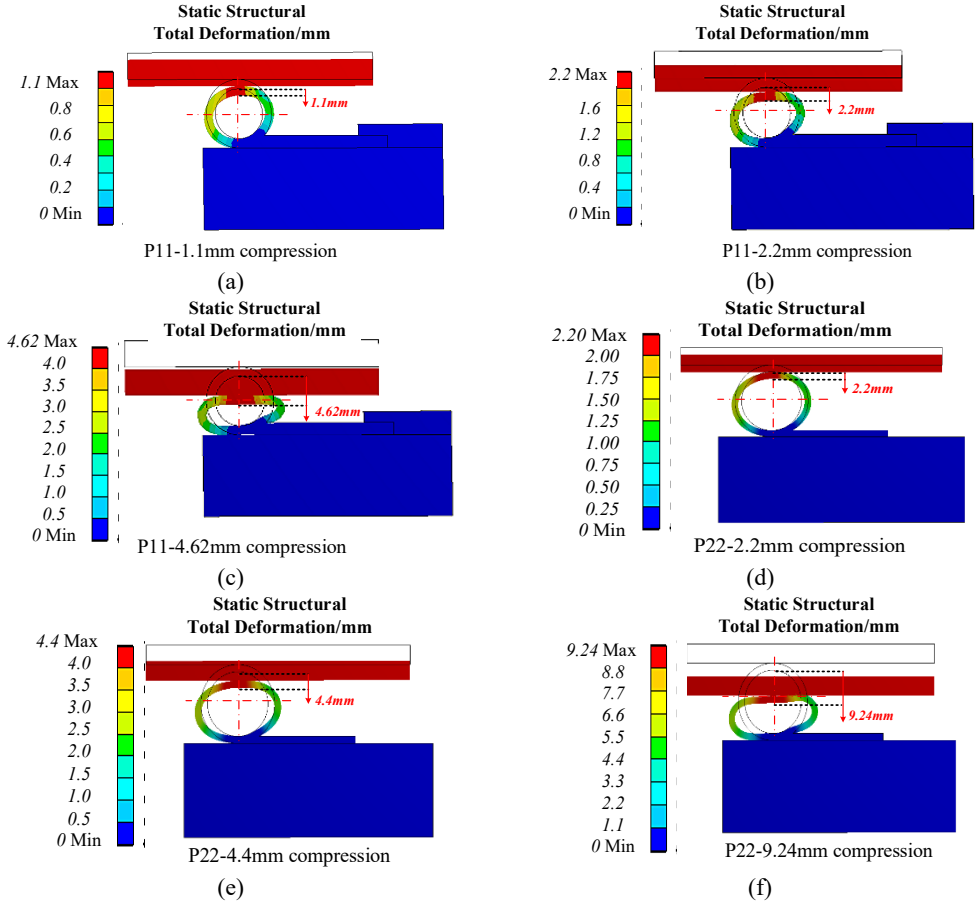

Fig.9. Cloud images of the compression deformation from finite element analysis

In Fig. 9, the black frame is the original outline of the P-shaped ring, and the cloud image shows the shape after compression and deformation. It can be seen that as the compression rate increases within a specific range, the deformation of the P-shaped sealing ring increases significantly. Moreover, the stress and strain value at the contact position of the sealing pair increases significantly, which improves the overall sealing performance of the device and reduces leakage. The stress-strain curves are shown in Fig. 10.

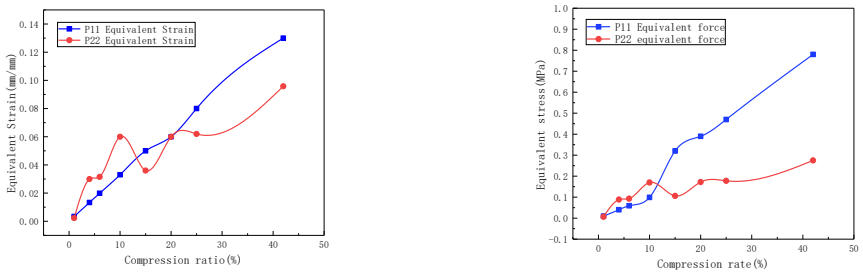

Fig.10. Stress-strain curve of the sealing ring

Compared with the general calculation method, the above simulation analysis considers the high nonlinearity of the rubber material and the anisotropy of the structure. Thus, it constructs a super-elastic model of the material. The curves show that the stress and strain values of the two sizes of P-shaped rubber seals under eight compression conditions are similar. This indicates that the seal leakage test can serve as a good reference for the same type of sealing test.

3 P-shaped heat seal structure and performance test

3.1 Leakage test under different compression rates

The high-temperature heat seal leakage tests for different compression rates are mainly divided into two groups. The first group of tests are for the P-shaped rubber sealing ring with a diameter of 22mm, and the second group of tests are for the rubber P-shaped rubber sealing ring with a diameter of 11mm. Each group of tests are carried out in two steps. The first step is a regular temperature test. The test is carried out under two pressures (6.9KPa/13.8KPa) and different compression rates without heating. The second step is a high-temperature test. Air and the backplane sealing ring are heated to the target temperature, and leakage test is performed under different compression rates and pressures similar to the normal temperature test. The compression rate is adjusted by changing the thickness of the positioning block. The test is finished when no leakage at a high temperature is found.

The results of the high-temperature heat sealing airtightness test of P22mm and P11mm sealing rings are shown in Fig. 11. Overall, the sealing performance of the two types of P-shaped rings at high temperatures is enhanced compared to the normal temperature conditions. The sealing performance of the sealing ring with an 11mm outer diameter is even better. The leakage of the sealing ring with 11mm outer diameter changes more linearly with the compression rate. Within a specific range, the leakage rate decreases linearly with the increase of the compression rate. The sealing ring with an outer diameter of 22 mm has a steep drop in the leakage rate with the compression rate increase. When the compression rate is 15%, there is no leakage under the two pressures for high and low temperatures. The surface of the sealing ring is made of fibre material, and there are many tiny gaps between the fibres, and gas can leak through these microchannels. As the compression rate increases, displacement and friction are produced within the fibre structure due to squeezing by the positive pressure. Consequently, the porosity decreases, the leakage micro-channels decreases, and the leakage volume also decrease.

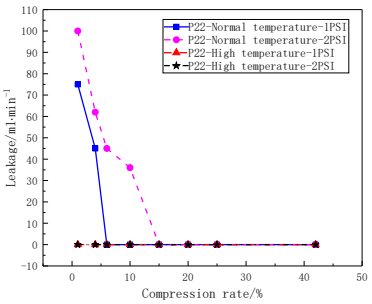

(a) Leakage curve of Test-1

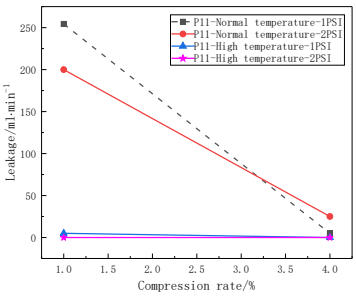

(b) Leakage curve of Test-2

Fig.11. Leakage curves of two samples with different compression rates

3.2 Leakage test with different number of openings

The test sample is a P-shaped rubber sealing ring with a 22mm diameter. Under fixed compression rate (4%), leakage test is performed on sealing rings with and without openings or multiple holes. The specific test steps are the same as in the case of the compression rate test. Tests are performed on the same P-shaped rubber ring without openings, with 4 openings and 8 openings to ensure consistency. In order to exclude the influence of other factors, only temperature and pressure are changed. Data are analyzed, and the law of the influence of the number of openings on the leakage is obtained. The test results are shown in Fig. 12.

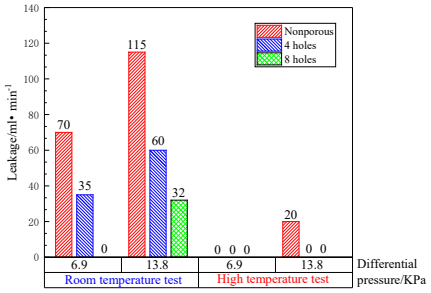

Fig.12. Leakage test results of the sealing ring with/without openings

It can be seen that the sealing effect under high temperature is better than that obtained under normal temperature, which satisfies the principle of thermal expansion and contraction. Under high temperature and 13.8 KPa pressure, as the number of openings increases, the leakage will decrease until there is no leakage. Under normal temperature, the leakage trends are similar under two pressure values. As the number of openings increases exponentially, the amount of leakage decreases approximately at the same rate. A certain number of openings has a positive impact on the sealing effect. The outer side of the sealing ring is opened in the circumferential direction. When the fluid enters the inner cavity of the sealing

ring, the pressure in the inner cavity of the sealing ring is increased. This expansion effect improves the supporting ability of the sealing ring, thereby reducing gas leakage. The specific principle is shown in Fig. 13.

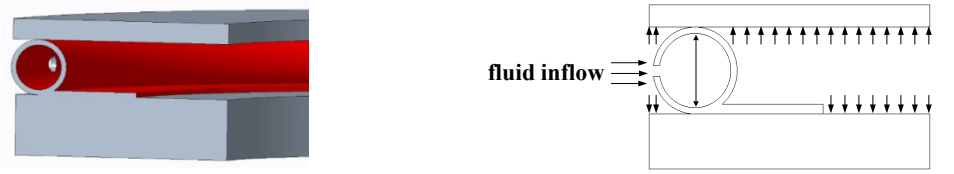

(a) 3D modeling of open-end seals (b) Sealing principle of sealing ring with openings

Fig.13. Fluid leakage through the sealing ring with openings

3.3 Comparative analysis of finite element simulation and field test results

For the finite element transient heat transfer analysis of the tester structure, the backplane is given a heat load boundary of a single heat source (200 °C), and the target temperature can be reached after 900 seconds. Infield tests reveal that the backplane is heated by high-temperature resistance wires made of phlogopite sheets. After about 14 minutes of heating, the E5EC temperature meter shows that the target temperature has been reached and stabilized. The filed test results are consistent with the simulation results.

In the 2D finite element compression simulation analysis, the equivalent stress and strain cloud images of the two types of the P-shaped ring are calculated for the given compression rates and compression distances. The results show that as the compression rate increases, the stress and strain values of the two types of sealing rings show an increasing trend. This indicates that the contact stress of the sealing contact surface (seal pair) increases with the increase of the compression, which is beneficial to enhance the overall sealing performance of the device. Moreover, the stress and strain value of the 11mm diameter sealing ring is higher than that of the 22mm diameter sealing ring. Therefore, the simulation shows that the sealing performance of the P11mm sealing ring is better. The infield tests indicate that the 11mm diameter seal leakage is zero under 4% compression rate, and there is no need to carry out later compression tests. On the contrary, the 22mm diameter seal maintains zero leakage under a 15% compression rate steadily. The infield test results are consistent with the simulation analysis, indicating that the simulation analysis methods have a significant guiding value for the field test.

4 Conclusion

This paper proposes a research method based on the combination of finite element modeling simulation and experimental test correlation verification for the testing of spacecraft thermal seal structure and leakage characteristics. The method firstly develops a test plan and builds a test control system for high-temperature thermal seal leakage characteristics based on the medium to be tested and the test target, then carries out the compression deformation simulation of the P-ring and the temperature field analysis of the tester tooling by means of finite element technology, and finally obtains the leakage data under different working conditions (temperature, pressure difference, compression rate) and different number of openings of the sealing medium structure by means of experimental tests. The following conclusions are drawn:

(1) In heat sealing test, real high-temperature conditions need to be simulated to characterize the sealing performance better. The test results show that the sealing performance under high-temperature is significantly better than that under normal-temperature working condition. Furthermore, the leakage rate is lower in the high-temperature working condition, and the sealing performance is better.

(2) The heat sealing test conditions need to cover different working and structural parameters. The test results show that the leakage rate of the P-shaped heat seals changes significantly under different compression rates, gas pressures, and different numbers of openings.

(3) With the development of hypersonic aircraft, high-temperature seals will face more demanding working environments, such as high temperature, high pressure, and high load. Therefore, the design of the heat-sealing test also needs to adapt to such changes and enhance the parameter design space.

REFERENCES

[1]. *Kang J.* Relevant Thinking on the Thermal Protection Technology of Hypersonic Aircraft Structure. ChinaArab Science and Technology Forum (Chinese and English),2020(09):87-89.
[2]. *Sun Yan*. Airborne Equipment Housing Seal Design. Machinery Management Development,2021,36(11):6-7.
[3]. *Yuan X X, Xiao K Y, Wu J*. Design of Hatch-door for Manned Near Space Vehicle. Manned space flight,2018,24(02):218-226.
[4]. *Xiao J, Liao Z Z, Zhang Z J,* et al. Resear-ch on the application of Thermal Seal an-d Convenient Maintenance Materials for High-Speed Airborne Missile. Aviation Weapons: 2022,1-6.
[5]. The Challenger bombing 17 years ago. Chinese Spaceflight,2003(03):2-6.

[6]. Manned plan, safety first, Columbia incid-ent caused major repercussions. Chinese Spaceflight,2003(03):11-14.
[7]. *Dunlap P H , Steinetz B M , Curry D M , et al*. Investigations of a Control Surface Seal for Reentry Vehicles. Journal of Spa-cecraft and Rockets, 2003.
[8]. *Oswald J J , Mullen R L , Dunlap P , et al.* Modeling and Evaluation of Canted Coil Springs as High Temperature Seal Preloading Devices. 2004.
[9]. *Steinetz B M , Hendricks R C* . Overview of NASA Glenn Seal Development Prog-ram. 2001.
[10]. *Taylor S C, Demange J J, Dunlap P, et al*. Further Investigations of High Temperat-ure Knitted Spring Tubes for Advanced Control Surface Seal Applications. Aiaa J-ournal, 2006.
[11]. *Oswald J J, Mullen R L, Dunlap P, et al*. Modeling and Evaluation of Canted Coil Springs as High Temperature Seal Preloa-ding Devices. 2004.
[12]. *Liu S,Man Y J,Ma W M,et al.* Research o-n the Influence of Compression Rate and Seal Pressure Difference on the Perform-ance of High Temperature Dynamic Seal. China Aerospace Third Professional Info-rmation Network, China Association for Science and Technology Aeroengine Ind-ustry-University Consortium (under preparation): China Aerospace Third Professi-onal Information Network,2019:5.
[13]. *Finkbeiner J , Dunlap P , Steinetz B , et al.* Investigations of Shuttle Main Landing Gear Door Environmental Seals // 41st AIAA/ASME/SAE/ASEE Joint Propulsion Conference & Exhibit. 2005.
[14]. *Steinetz B M.* Seal Technology for Hyper-sonic Vehicles and Propulsion Systems: An Overview. 2008.
[15]. *He Jun, Li Ying, Yu R, et al.* A Practical Research on Flexible Graphite on High T-emperature Seal of Solid Rocket Motor. Journal of Ballistic Arrows and Guidance,2020,40(06):1-4.
[16]. *Wang Yulong*. Research on the testing te-chnology of metal-wound gasket sealing performance under high temperature and pressure environment. Changchun Univer-sity of Science and Technology,2021.
[17]. *Qiu B*. Numerical simulation study of vor-tex structure and thermal environment in-side the transverse gap of hypersonic ve-hicle. China Aerodynamics Research and Development Center,2015.
[18]. *Tang G M*. Experimental study on heat tr-ansfer of control wing slit flow. Acta Ae-rodynamics,1989(01):88-93.
[19]. *Huang F, Liu R S, Ke Y C, et al*. Finite E-lement Simulation of Compression Beha-vior for Rubber Seal. Aviation Manufact-uring Technology, 2013(06): 83-88.
[20]. *Bai Y G, Xia G Q, Sun D C, et al*. Resear-ch on numerical method of heat-sealing structure for spacecraft hull based on mul-tiphysics coupling. Solid rocket technolo-gy, 2014, 37(06): 756-762.
[21]. *Qiu C T, Chen Z Z*. Study of Thermalstru-cture Design and Analysis for Hypersoni-c Vehicles. Aircraft design, 2012, 32(06): 6-14.
[22]. *Li J N.* Analysis and design of mechanica-l properties of elastic elements in heatse-aled structure. Harbin Institute of Technol-ogy,2020.
[23]. *Lu W, Zhong Q, Huang J R, et al*. Resear-ch on heat leakage in the sealed compart-ment of manned spacecraft. Journal of As-tronautics, 2012, 33(002): 145-152.
[24]. *X.W. Sun*. Hypersonic aerodynamic ther-mal prediction and thermal protection ma-terial/structure response study. Universit-y of Science and Technology Beijing, 20-20.
[25]. *Liu Y, Zhang Y, Zhao F, et al*. Simulation analysis of steady-state and transient temperature field of Electromagnet for fuel pump system. Microelectromechanics,2019,52(09):46-49+55.
[26]. *Wang Z F, Gao Y, Xu X L, et al*., Design Method and Performance Evaluation Crit-eria of Advanced Spacecraft Heat Seal. J-ournal of Astronautics, 2018, 39(07): 793-800.
[27]. *Yi Zheng, Dai Yanbin, Yang Jianchang, et al.* Temperature field analysis of laser irradiated optical windows. Laser and Infrared, 2022, 52(02): 259-265.

[28]. *Bai Y G, Xia G Q, Sun D C, et al*. Resear-ch on numerical method of heat-sealing structure for spacecraft hull based on mul-tiphysics coupling. Solid rocket technolo-gy, 2014, 37(06): 756-762.
[29]. *Li X F, Yang X X.* A review of elastic con-stitutive model for rubber materials. Elas-tomer, 2005, (01): 50-58.
[30]. *Hou Wan, Chen Huilong, Cheng Qian, et al.* Numerical calculation and analysis of vapor-liquid-solid flow characteristics of high temperature sealing lubricating film. Chemical Progress: 2022,1-16.
[31]. *Liu J L, Xu Z G, Zhang F, et al*. High tem-perature sealing performance of braided heat-sealed components. Journal of Textil-es, 2021, 42(10): 84-91.
[32]. *Xue Yunjia, Liu Jiachen*. Preparation of F-lexible Fiber Blankets and Their Elastici-ty and Thermal Insulation Properties, 20-22, 23(03): 1-13.
[33]. *Ke Y C.* Research on Key Performances a-nd Molding Process of Aviation Rubber Sealing Structure. Tsinghua University,20-16.
[34]. *Liu Yanjun, Wu Guofeng*. Leakage model study of metal O-ring seal structure. Lubrication and Seals, 2019, 44(9):19-24.
[35]. *Xu Tongjiang*. Finite element analysis of O-shaped seal based on ANSYS. Shando-ng University, 2012.
[36]. *Guo Aimin, Liu Weiwei, Peng Bo, et al*. Decoupling solution method for vehicle h-atch seal load. Missile and Space Launc-h Technology, 2018(4): 18-21.
[37]. *Han C R*. The Theory of Finite Deformati-on and Its Application in Geotechnical E-ngineering. Graduate School of Chinese Academy of Sciences (Wuhan Institute of Rock and Soil Mechanics), 2009.